

## Potential overestimation of community respiration in the western Pacific boundary ocean: What causes the putative net heterotrophy in oligotrophic systems?

Yibin Huang <sup>1,2</sup> Bingzhang Chen,<sup>3</sup> Bangqin Huang <sup>1,2\*</sup> Hui Zhou,<sup>4,5,6</sup> Yongquan Yuan<sup>5,7,8</sup>

<sup>1</sup>State Key Laboratory of Marine Environmental Science, Xiamen University, Xiamen, China

<sup>2</sup>Fujian Provincial Key Laboratory of Coastal Ecology and Environmental Studies, Xiamen University, Xiamen, China

<sup>3</sup>Department of Mathematics and Statistics, University of Strathclyde, Glasgow, United Kingdom

<sup>4</sup>CAS Key Laboratory of Ocean Circulation and Waves, Institute of Oceanology, Chinese Academy of Sciences, and Pilot National Laboratory for Marine Science and Technology, Qingdao, China

<sup>5</sup>Center for Ocean Mega-Science, Chinese Academy of Sciences, Qingdao, China

<sup>6</sup>University of Chinese Academy of Sciences, Beijing, China

<sup>7</sup>Key Laboratory of Marine Ecology and Environmental Sciences, Institute of Oceanology, Chinese Academy of Sciences, Qingdao, China

<sup>8</sup>Laboratory for Marine Ecology and Environmental Science, Pilot National Laboratory for Marine Science and Technology, Qingdao, China

### Abstract

Microbial metabolism is of great importance in affecting the efficiency of biological pump and global carbon cycles. However, the metabolic state of the oligotrophic ocean, the largest biome on Earth, remains contentious. We examined the planktonic and bacterial metabolism using *in vitro* incubations along the western Pacific boundary during September and October 2016. The integrated gross primary production (GPP) of the photic zone exhibited higher values in the region of 2°–8°N along 130°E and the western Luzon Strait, which is consistent with the regional variability of nutrients in the different ocean provinces. Spatially, the community respiration (CR) was less variable than the GPP and slightly exceeded the GPP at most of the sampling stations. Overall, the *in vitro* incubation results suggest a prevailing heterotrophic state in this region. A comparison of the metabolic rates from the *in vitro* incubations with recently published biogeochemical model results in the same region shows that our observed GPP values were close to those predicted by the model, but the measured CR was approximately 30% higher than the modeled values. We also found that most of the *in vitro* CR estimates were higher than the upper range of the empirical CR estimated from the sum of the contributions of the main trophic groups. Conversely, the estimates of the empirical CR support the rationality of the CR predicted by the biogeochemical model. In general, the results indicate that systematic net heterotrophy is more likely a result of the overestimation of CR measured by the light–dark bottle incubation experiments, although the exact cause of the methodological problem remains unknown.

Biological carbon production and consumption are two important ecological processes in the marine system and contribute significantly to the global carbon cycles (Longhurst 1995). Marine phytoplankton are responsible for almost half of global primary production (Field et al. 1998). Most of the organic carbon produced via photosynthesis is remineralized by heterotrophic organisms and released as dissolved inorganic carbon, and a tiny fraction of the particulate organic carbon is exported into the deep

ocean, which is the so-called biological pump process (Sigman and Boyle 2000). The difference between the gross primary production (GPP) and community respiration (CR), termed net community production (NCP), should theoretically be equal to the amount of organic carbon available for potential export and thus is suggested to be one of the best descriptors of the role of biota in oceanic absorption or release of atmospheric CO<sub>2</sub> (Ducklow and Doney 2013). Increasing amounts of evidence indicate that in addition to primary production, the variability and magnitude of heterotrophic respiration also play important roles in the emergence of the geographic patterns of NCP or export production (Aranguren-Gassis et al. 2011; Serret et al. 2015). Therefore, accurate assessments of autotrophic and heterotrophic metabolism are required

\*Correspondence: bqhuang@xmu.edu

Additional Supporting Information may be found in the online version of this article.

for a more comprehensive understanding of the efficiency of the biological pump at the global scale.

Over the last several decades, the metabolic state in the oligotrophic ocean has been actively debated in oceanography; the NCP signals derived from the *in vitro* incubation approach, typically using light–dark bottles, suggest a prevalence of heterotrophy in the oligotrophic ocean, which is in sharp contrast with the consistently positive NCP signals derived from incubation-free methods (Duarte et al. 2013; Ducklow and Doney 2013; Williams et al. 2013). The advantage of the incubation approach is that it allows us to estimate the integrated NCP from discrete depths and over 24 h, whereas most incubation-free techniques can only constrain the integrated rates at fixed depths, typically within the surface mixed layer. Duarte et al. (2013) compiled a global incubation-based data set, and the scaling functions suggest that the open ocean, with values of GPP and chlorophyll *a* (Chl *a*) concentrations less than  $2 \text{ mmol O}_2 \text{ m}^{-3} \text{ d}^{-1}$  and  $0.44 \text{ mg m}^{-3}$ , respectively, tends to be systematically heterotrophic. In addition, Regaudie-de-Gioux and Duarte (2012) examined the sensitivity of primary production and respiration to temperature, and the results implied higher activation energy of respiration ( $0.66 \pm 0.05 \text{ eV}$ ) than primary production ( $0.32 \pm 0.04 \text{ eV}$ ). The implication is that all other things being equal, the CR is likely to exceed the GPP in the tropical and subtropical ocean. However, the purported heterotrophy suggested by *in vitro* incubation remains questionable in part because the carbon deficit is difficult to sustain based on the current understanding of ocean carbon cycling (Ducklow and Doney 2013; Williams et al. 2013). Recent improvements in understanding this controversy were attempted by Letscher and Moore (2017), who first included globally optimized dissolved organic carbon cycling into an ecosystem-circulation ocean model to assess the metabolic rates around the global ocean, which provides a powerful approach to validate the observations of the metabolic state from a geochemical perspective.

Bacteria play a vital role in the nutrient and organic cycle (Arrigo 2005) and mediate the carbon transfer efficiency from lower to higher trophic levels through the microbial loop, which in turn influences the organic export (Azam et al. 1983; Jiao et al. 2010). Bacterial respiration has been commonly considered to be the major part of CR. Especially in some unproductive marine ecosystems, bacterial respiration has been suggested to even exceed the net primary production (Del Giorgio et al. 1997). However, this view was challenged by Calbet and Landry (2004), who argued that because microzooplankton consume a substantial proportion (~70%) of primary production, their contribution to CR must not be negligible. Thus, quantification of bacterial activity is critical for defining the metabolic balance.

The western Pacific Ocean is a particularly important region in regulating the global ocean circulation and climate system by the active exchange and transport of water, heat, and salinity with adjacent tropical and subtropical oceans (Hu et al. 2015). The currents in the epipelagic zone are complicated and mainly include the North Equatorial Current (NEC),

North Equatorial Countercurrent, Subtropical Countercurrent (STCC), Kuroshio Current (KC), and Mindanao Current (MC) (Hu et al. 2015). This area is a water-mass crossroads (Fine et al. 1994) and is also a typical tropical-subtropical oligotrophic environment that is characterized by very low Chl *a* and nutrient concentrations in the upper ocean (Yang et al. 2017c). The present knowledge about this region is particularly focused on the hydrographic dynamics (see the review of Hu et al. 2015), and the biological processes have been explored much less except for several reports on the geographic patterns of zooplankton distributions (Yang et al. 2017b) and nitrogen fixation (Shiozaki et al. 2009). The aim of this study is to determine the geographic pattern of planktonic and bacterial activity in the region of the still under-sampled western Pacific boundary. Although incubation experiments using light–dark bottles are a straightforward and widely used method to measure metabolic rates in various environments, the different results in the oligotrophic ocean between this method and other incubation-free methods suggest that there might be a bias with this method, particularly in oligotrophic warm oceans (Duarte et al. 2013; Williams et al. 2013). Of course, each methodology has its own assumptions and potential limitations. It is desirable to compare methods to reduce the uncertainty and enhance our understanding of the metabolic state of the oligotrophic ocean, which is the largest biome on Earth. Specifically, we compare our observational results with those of an excellent modeling study of the metabolism of the global ocean (Letscher and Moore 2017). We also try to estimate CR by summing the contributions of major trophic groups based on independent measurements and various conversion factors (CFs) reported in the literature.

Based on these arguments, we ask the following two sets of questions:

1. Can we observe the net heterotrophic state in the tropical-subtropical and oligotrophic western Pacific boundary using the *in vitro* incubation method following the scaling laws proposed by Duarte et al. (2013)? Will the results be consistent with the model results of Letscher and Moore (2017) and other estimates? If the answers are yes, then we should search for evidence of lateral transport of dissolved organic matter in this region.
2. If the estimated NCP rates differ between methodologies, what are the sources in terms of the GPP or CR that cause this discrepancy? In other words, what types of measurements are the most likely to be biased?

## Methods

### Study sites

The cruise was conducted in the western North Pacific Ocean along two transects at  $130^\circ\text{E}$  ( $2^\circ\text{N}$ – $20^\circ\text{N}$ ) and  $20^\circ\text{N}$  ( $120^\circ\text{E}$ – $132^\circ\text{E}$ ) from 07 September 2016 to 09 October 2016, on RV “KEXUE” (Fig. 1). A total of 31 stations was investigated, and

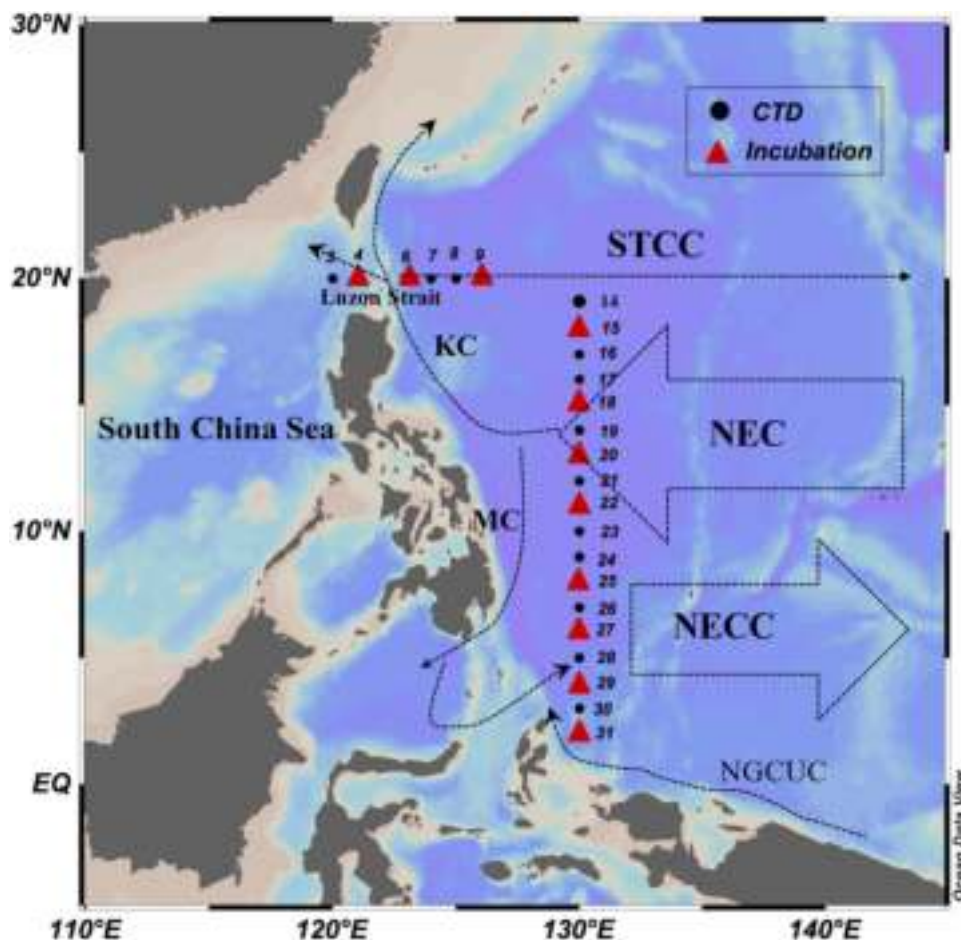


**Fig. 1.** Map of sampling stations in the western Pacific Ocean during September and October 2016. The dotted lines represent the approximate regions of the main currents in the western Pacific Ocean. The red triangles indicate locations where planktonic and bacterial metabolism were measured. KC, Kuroshio current; MC, Mindanao current; NEC, north equatorial current; NECC, north equatorial countercurrent; NGCUC, New Guinea coastal undercurrent; STCC, subtropical countercurrent. [Color figure can be viewed at [wileyonlinelibrary.com](http://wileyonlinelibrary.com)]

11 stations were used for incubation experiments (red triangles in Fig. 1). The approximate fields of the main currents in the western North Pacific are shown in Fig. 1.

#### Physical and chemical measurements

The water temperature and salinity at each station were measured using a Sea-Bird Electronics CTD SBE 911plus probe. The conductivity, temperature, and depth probes (CTD) was calibrated immediately before the cruise. To determine the concentrations of inorganic nitrate plus nitrite, ammonium and silicate and phosphate, 100 mL water samples were collected at 6–8 discrete depths from 0 to 300 m using 20-liter Niskin metal-free bottles attached to the rosette of the CTD. The water samples were subsequently analyzed using a Skalar Flow Analyzer (Skalar, The Netherlands), and the data quality was estimated via intercalibration. The depth of the nitracline was determined as the depth where the nitrate concentration reached  $5 \text{ mmol m}^{-3}$ . The nitrate gradient across the base of the euphotic zone at each station was calculated as an index of the potential availability of nutrients in the euphotic zone by vertical diffusion from the deeper layer.

#### Biological measurements and in vitro oxygen-based metabolism

Seawater samples from five discrete depths, corresponding to 100%, 50%, 10%, and 1% of the surface incident irradiance and the deep chlorophyll maximum (DCM), were collected at the incubation stations above 200 m water depth before dawn. If the depth of the DCM was coincident with the depth of 10% or 1% surface incident irradiance, an additional depth between the layers of 50% and 1% surface incident irradiances was sampled. The sampled water was transferred into 10-liter acid-cleaned carboys using a silicone tube. One liter of water was filtered onto a Whatman GF/F filter to measure the Chl *a* concentration. The Chl *a* was extracted using 90% aqueous acetone in dark conditions for 12–20 h at 4°C and then measured by a Turner Trilogy fluorometer (Welschmeyer 1994).

The planktonic community metabolic rates were estimated from the changes in dissolved oxygen concentrations in the light–dark bottles over a 24-h incubation period following the procedure of Serret et al. (1999). The dissolved oxygen concentrations were determined by high-precision Winkler titration

(Oudot et al. 1988; Huang et al. 2018) with an automated potentiometric end-point detection system (Metrohm-848, Switzerland). For each depth, the water samples were carefully siphoned into 12 calibrated 100 mL borosilicate bottles using silicon tubing, with more than 300 mL overflowing. Then, four replicate bottles were immediately fixed by the Winkler reagents with  $\text{MnCl}_2$  ( $3 \text{ mol L}^{-1}$ ) and  $\text{NaI}$  ( $4 \text{ mol L}^{-1}$ )/ $\text{NaOH}$  ( $8 \text{ mol L}^{-1}$ ) to quantify the initial dissolved oxygen concentrations. The four light bottles were covered by neutral density meshes to adjust the light conditions to mimic the in situ irradiances of the corresponding sampling depths. The remaining quadruplicate bottles were placed inside dark bags as dark bottles. Both the light and dark bottles were incubated in a large tank on the deck filled with running seawater pumped from the surface ocean and exposed to natural sunlight. After the 24-h incubation period, the dissolved oxygen concentrations in the bottles were determined. GPP was calculated as the difference between the average dissolved oxygen concentrations in the light and dark bottles, and CR was calculated as the difference between the average dissolved oxygen concentrations in the initial and dark bottles. NCP was equal to  $\text{GPP}-\text{CR}$ . The average percentage coefficients of variation (% ratio of the standard deviation to the mean) of the dissolved oxygen replicates were 0.15%, 0.17%, and 0.17% for the initial, light, and dark bottles, respectively. The complete data set will be deposited in the public global respiration database: <https://www.uea.ac.uk/environmental-sciences/people/profile/carol-robinson#researchTab> (the data set is maintained by Carol Robinson).

We noted that the on-deck incubation is subject to some problems such as changes of in situ light and temperature conditions for the submarine samples during the incubation. The metabolic rates are temperature-dependent (López-Urrutia et al. 2006; Regaudie-de-Gioux and Duarte 2012). The temperature in the incubator maintained by the running surface seawater would artificially elevate the in situ temperature conditions for the subsurface samples during the incubation. To minimize this effect, the metabolic rates below the surface were corrected by the activation energy of the GPP and CR reported by Regaudie-de-Gioux and Duarte 2012 (Supporting Information). It is also well known that the spectral characteristics of submarine light differ from those of surface light, featured with a higher fraction of blue light (Clarke and Oster 1934). The use of neutral density screen in our study well simulated the attenuation of submarine light intensity, but failed to simulate submarine spectral composition. Since the peak absorption bands of most algal pigments lie in the blue region of the visible light spectrum, the Chl *a*-specific absorption coefficient for the phytoplankton in the subsurface ocean would be higher in the same intensity dominated by blue light than white light. A previous study of Laws et al. (1990) showed that real primary production rates would be underestimated by a factor of two if incubations are performed using surface light attenuated with neutral density screen. In

the present study, the sampling depths were identified as different gradients of broadband surface light estimated by the depth-averaged attenuation coefficient of water column ( $K_{\text{mean}}$ ). A study by Kyewalyanga et al. (1992) suggested that water-column primary production integrated from the sampling depths determined by  $K_{\text{mean}}$  was not significantly different from the real primary production. Their results indicated that light field judged by  $K_{\text{mean}}$  criterion gave higher light intensity at all depths compared to light intensity calculated using the spectral light value, then resulting in overestimating the in situ primary production. Thus, the negative bias due to the difference of spectral characteristics in the submarine would be partly compensated by the positive bias inherited from overestimated light intensity, leading to a final integrated value of primary production close to the real primary production. In the future study, more improvements are expected to accurately achieve ambient in situ condition and reduce the uncertainty by using the neutral and blue density screen or the incubation buoy.

### Bacterial production

Bacterial production (BP) was measured followed the protocols of  $^3\text{H}$ -leucine incorporation (Kirchman 1993; Chen et al. 2014). Four 1.8-mL aliquots of water were collected from each depth and added to 2-mL sterile microcentrifuge tubes (Axygen, U.S.A.), and they were incubated with a saturating concentration ( $10 \text{ nmol L}^{-1}$ ) of  $^3\text{H}$ -leucine (Perkin Elmer, U.S.A.) for 2 h in the dark. One sample was immediately killed by adding 100% trichloroacetic acid (TCA) as a control, and the other three incubations were stopped by the addition of TCA at the end of the 2-h incubation. Five vacuum cups filled with the seawater from the corresponding sampling depths were used as the incubators for BP to stimulate the in situ temperature during the 2-h incubation. After the incubation, the water samples were filtered onto  $0.2\text{-}\mu\text{m}$  polycarbonate filters (GE Water & Process Technologies, U.S.A.). The filters were rinsed twice with 3 mL of 5% TCA and twice with 2 mL of 80% ethanol before being frozen at  $-20^\circ\text{C}$ . Upon return to the laboratory, the dried filters were placed in scintillation vials with 5 mL of Ultima Gold scintillation cocktail (Perkin-Elmer, U.S.A.). The radioactivity retained on the filters was measured as disintegrations per minute using a Tri-Carb 2800TR liquid scintillation counter (Perkin Elmer, U.S.A.). The rate of incorporation of  $^3\text{H}$  leucine was calculated from the difference between the treatment and control tubes.

Seven experiments were conducted to determine empirical factors to convert from the leucine incorporation rates to bacterial carbon production. Predator-free water was obtained by filtering seawater through  $1\text{-}\mu\text{m}$  polycarbonate membrane filters and then diluted to 10% by  $0.2\text{-}\mu\text{m}$  filtered seawater. The leucine incorporation rates and bacterial abundance were monitored every 4–6 h for a maximum of 2 d. The cumulative method was used to derive the empirical CF by linear regression of the bacterial number yields against the integrated

leucine incorporation rates (Bjørnsen and Kuparinen 1991). The factor of 30.2 fg C cell<sup>-1</sup> was applied to convert bacterial abundance to carbon biomass (Fukuda et al. 1998). The CFs in our measurements varied from 0.20 to 0.91 kg C mol Leu<sup>-1</sup>, and we used the geometric mean value of 0.37 kg C mol Leu<sup>-1</sup> to convert the incorporation of leucine to carbon units.

### Integrated metabolism rates derived from the biogeochemical ocean model

The model-based metabolism used in our study was based on the results derived from a recently published biogeochemical model in the same region (Letscher and Moore 2017). We chose this model because the organic carbon concentrations are well calibrated in the model. In Letscher and Moore (2017), three types of allochthonous organic carbon sources (contemporary rivers, atmospheric deposition, and realistic semi-labile and refractory marine dissolved organic carbon pool) were integrated into the Biogeochemical Elemental Cycling v1.2.2 module of the Community Earth System Model. The model outputs include both GPP and CR within the euphotic zone, which allows us to directly compare them with our measured values from the light–dark bottles. In addition, the physical forcing of the western Pacific boundary has been well resolved in the ecosystem-circulation model; therefore, we feel confident that the results in this region would be reasonable.

Briefly, the GPP in this model was computed from the phytoplankton nitrogen demand satisfied by nitrate, ammonium, and N<sub>2</sub>-fixation. CR was calculated as the sum of the carbon losses induced by the mortality of phytoplankton and zooplankton, phytoplankton grazed by zooplankton, and respiration of both particulate and dissolved organic carbon. Therefore, NCP is equal to GPP minus CR. The horizontal resolution of the model outputs is 1° × 1° with a higher resolution near the equator. The vertical resolution is 10 m in the upper 160 m. The daily volumetric metabolism (GPP and CR) from the model output is monthly climatology with 20-yr averages (1946–2007) in units of mmol O<sub>2</sub> m<sup>-3</sup> d<sup>-1</sup>. The integrated euphotic GPP and CR were calculated by trapezoidal integration of the volumetric data from the surface to the depth of 1% incident irradiance (typically 100–120 m in this study). Because our study was conducted between September and October, we compared our results with the model outputs for both September and October. The spatial variations of the euphotic zone integrated GPP and CR in this region are presented in Supporting Information Fig. S2. To conduct a paired comparison of the metabolism at each sampling station, we extracted the volumetric GPP and CR from the biogeochemical model in the corresponding grid cells within which our sampling stations were located.

### Estimates of the empirical CR from the contributions of different plankton groups

Because our measured GPP values are consistent with the model results from Letscher and Moore (2017) (see “Results” section), we are confident in the GPP estimations in this area

and attempt to estimate the respiration rates of major groups based on the GPPs and published growth efficiencies of corresponding groups to provide additional constraints on the CR (Robinson et al. 2002; Robinson and Williams 2005; Morán et al. 2007). Mesozooplankton are usually considered to be poorly sampled by in vitro procedures in small volumes (i.e., 100 mL in this study) because of their low abundances. Therefore, we assume that the major groups in our incubation system are composed of heterotrophic bacteria, phytoplankton (dominated by *Prochlorococcus* and *Synechococcus*), and microzooplankton. Considerable errors are associated with the estimates of each group, but importantly, the results showed that even under the conditions of the maximum possible contributions, it is still difficult to bridge the gap between the in vitro measured respiration and the estimated respiration.

For phytoplankton respiration, Carvalho et al. (2017) reported that the global new respiration (which is mainly contributed by phytoplankton) ranges from 10% to 30% of GPP and that the remainder of the respiration (namely, old respiration) is contributed by other groups, including phytoplankton. If phytoplankton account for part of the old respiration as well, the corresponding ratio of phytoplankton respiration to GPP would be similar to the published ratio (–35%) (Duarte and Cebrián 1996). In a lab experiment, Marra and Barber (2004) observed that phytoplankton respired up to 40% of daylight primary production when exposed to 12:12 h light : dark conditions. Therefore, it is reasonable to constrain the possible range of phytoplankton respiration assuming a range of 15–40% of daily GPP. Based on a meta-analysis of grazing rates around the global ocean, Calbet and Landry (2004) suggested that approximately 50–60% of the GPP in the oligotrophic ocean is grazed by microzooplankton. The growth efficiency for protozooplankton and metazooplankton is generally considered to be in the range of 50–70% based on allometric scaling of protistan growth and respiration rates (Fenchel and Findlay 1983) as well as direct assessments from protistan carbon budgets (e.g., Verity 1985). We also compared three previously reported empirical functions that related the bacterial growth efficiency (BGE) to temperature (Rivkin and Legendre 2001), Chl *a* (López-Urrutia and Morán 2007), and BP (Roland and Cole 1999). Irrespective of the different assumptions, the resulting values of these three BGEs in our study were strongly correlated and yielded average values of 7.41% ± 0.03% for the temperature-based BGE, 7.93% ± 0.02% for the Chl *a* based BGE, and 9.09% ± 0.01% for the BP-based BGE (Supporting Information Table S1). These estimated BGEs are very similar to the in situ measured BGEs in the offshore stations of the North Atlantic, which have a mean value of 9% (Alonso-Sáez et al. 2007). Another uncertainty associated with the estimation of the bacterial respiration is CF, which is a crucial parameter for estimating BP and the additional impact on the magnitude of the estimated respiration contributed by bacteria. Our measured CFs varied by a factor of 4.5 (0.2–0.9 kg C mol Leu<sup>-1</sup>) with a mean value of 0.37 kg C mol Leu<sup>-1</sup>. Admittedly, applying a single mean value of the CF to estimate BP might bias the estimate of bacterial respiration.

**Table 1.** Estimates of the empirical community respiration contributed by major trophic groups.

| Trophic group          | Definition     | Methods                            | References                                      |
|------------------------|----------------|------------------------------------|---|
| Phytoplankton          | Upper boundary | Resp = 0.34 * GPP                  | Carvalho et al. (2017); Marra and Barber (2004) |
|                        | Lower boundary | Resp = 0.15 * GPP                  | Duarte and Cebrián (1996)                       |
| Microzooplankton       | Upper boundary | Resp = 0.65 * 0.7 * GPP            | Calbet and Landry (2004); Straile (1997)        |
|                        | Lower boundary | Resp = 0.5 * 0.5 * GPP             | Fenchel and Findlay (1983); Verity (1985)       |
| Heterotrophic bacteria | Upper boundary | Resp = (BP/0.07) – BP; (CF = 0.90) | López-Urrutia and Morán (2007)                  |
|                        | Lower boundary | Resp = (BP/0.09) – BP; (CF = 0.2)  | Rivkin et al. (2001); Roland and Cole (1999)    |

BGE, bacterial growth efficiency; BP, bacterial production; CF, conversion factor; GPP, gross primary production; Resp, respiration. Details about the calculations are described in the text.

Based on the studies described above, we attempted to constrain the upper and lower boundaries of the empirical CR at the sampling stations (Table 1). To quantify the upper boundary of the empirical CR, we assumed the case with values of 40% of daily GPP respired by phytoplankton, 60% of daily GPP grazed by zooplankton, 50% zooplankton growth efficiency, 0.9 kg C mol Leu<sup>-1</sup> of CF, and 7.4% of BGE in this region. Correspondingly, we constrained the lower boundary of the empirical CR by assuming that 15% of daily GPP is respired by phytoplankton, 30% of daily GPP is grazed by zooplankton, the zooplankton growth efficiency is 70%, CF is 0.2 kg C mol Leu<sup>-1</sup>, and BGE is 9.1% in this region.

### Statistical analysis

The rates integrated over the euphotic zone were calculated by trapezoidal integration of the volumetric data from the surface to the depth of 1% incident irradiance. The standard errors for the integrated values were estimated by the propagation procedures for independent measurements described by Miller and Miller (1988). We used a respiratory quotient of 1.2 to convert the carbon-based metabolism to an oxygen basis based on the assumption that inorganic nitrogen was released from organic matter in the form of ammonium (Laws 1991; Hedges et al. 2002). All GPP, CR, NCP, and BP values are presented as mean values with standard error. The data were log-transformed to satisfy the assumption of normality, which was confirmed (after transformation) via a Kolmogorov–Smirnov test. The correlations between the variables were examined by Pearson correlation. The linear regressions between the GPP and CR were conducted by reduced major axis regression analysis (model II linear regression) using the R software (R Core Team 2014). The spatial variabilities of GPP and CR were evaluated by calculating the coefficient of variation (% ratio of the standard deviation to the mean) of the integrated metabolism between the stations. The paired *t*-test was conducted to examine the difference between the metabolism rates at each sampling station derived from the O<sub>2</sub>-based incubation and the geochemical model predictions. The significance was satisfied if the type I error rate (*p*) was less than 0.05. Figs. 1–2 were plotted using the Ocean Data View software (Schlitzer 2012).

## Results

### Physical parameters and biochemical characterizations of the two transects

The characteristics of the potential temperature and salinity in the upper 300 m for each station are shown in Fig. 2. In this region, the water masses were relatively complicated due to the interactive influences of different currents. In the southernmost stations (Sta. 29–31), we observed higher salinity (> 35.25) at 200–300 m (Fig. 2a). This high salinity water originated from the South Pacific Tropical Water (SPTW) and was carried by the New Guinea Coastal Current and the New Guinea Coastal Undercurrent (NGCUC) from the South Pacific (Qu et al. 1999; Zhou et al. 2010). At Sta. 17–28, the upper water masses were mainly influenced by the typical North Pacific Tropical Water and were characterized by salinities slightly lower (34.75 < *S* < 35.25) than the SPTW (Fig. 2b,c; Fine et al. 1994; Qu et al. 1999). Sta. 14–16 were located along the boundary between the NEC and the STCC, where energetic meso-scale eddies were very active, and the water masses in this region have both tropical and subtropical gyre characteristics (Fig. 2c). On the transect along 20°N, the water masses at Sta. 5–9 were dominated by the Kuroshio water, which featured higher salinity and temperature than the water in the adjacent South China Sea (Fig. 2d). At Sta. 3 and 4, the upper water was a mixture of relatively fresh and cold water from the South China Sea and saltier and warmer water from the intrusion of the KC at depths of 200–300 m (Fig. 2d).

The main hydrographic features along the two transects are shown in Fig. 3. The water along the 130°E transect was characterized by high surface temperatures with a mean value of 29.8 ± 0.2°C. The surface salinity along this transect generally increased from 33.8 at the southernmost station (31) to 34.4 at Sta. 14. On the transect along 20°N, the temperature and salinity exhibited a westward trend toward colder and less saline waters. The average surface temperature along the 20°N transect (28.4 ± 0.2°C) was slightly lower than that along the 130°E transect. The lowest salinity along the 20°N transect was observed at the westernmost station (Sta. 4).

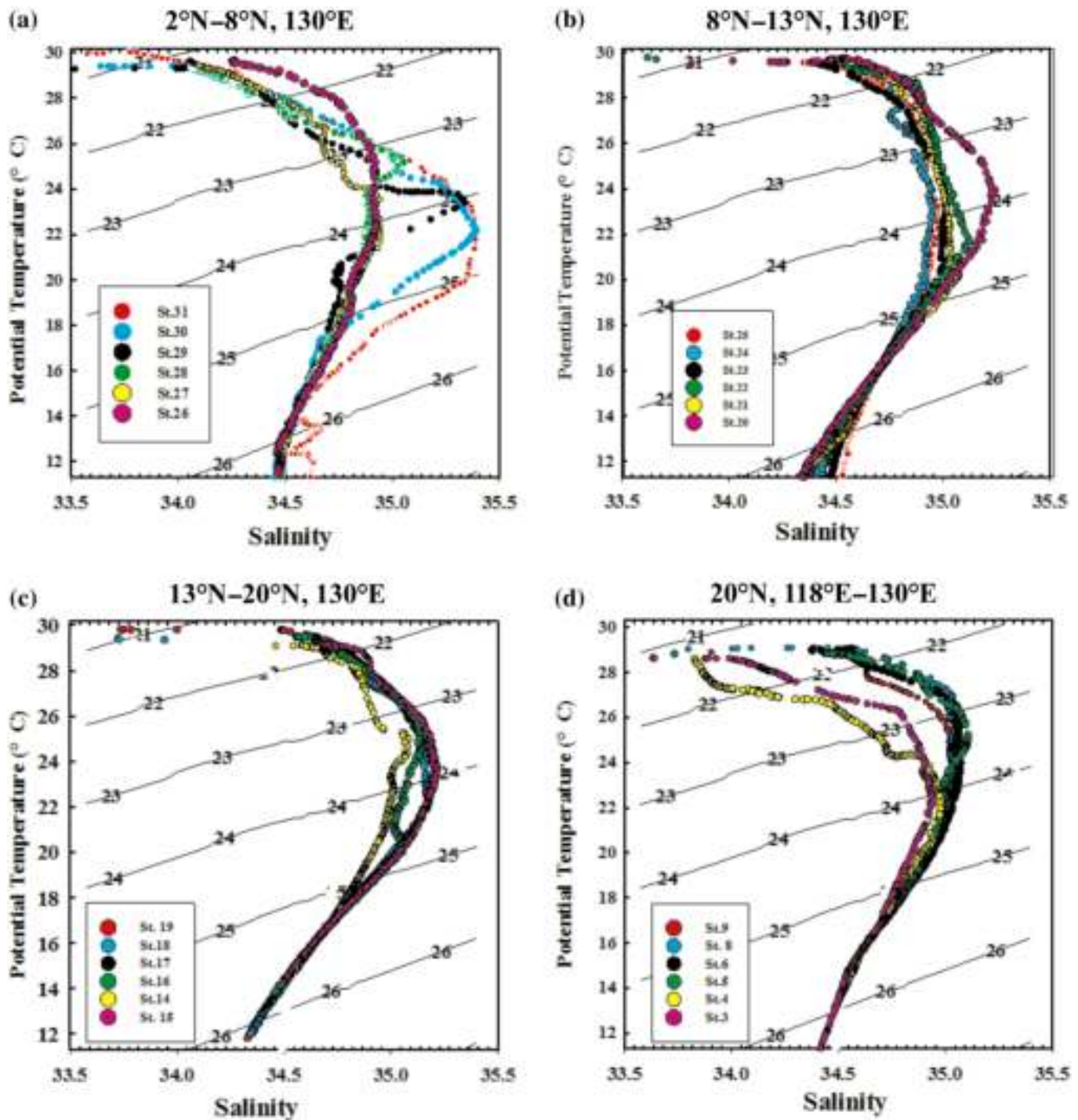


**Fig. 2.** Temperature-salinity diagrams (upper 300 m of water) of the sampling stations in the western Pacific Ocean. Black contours indicate  $\sigma_\theta$  (units: potential density- $1000 \text{ kg m}^{-3}$ ). Different colors represent different stations. [Color figure can be viewed at [wileyonlinelibrary.com](http://wileyonlinelibrary.com)]

The depths of the euphotic zone in the two transects (white lines in Fig. 3) were generally at approximately 100–150 m. Along the 130°E transect, the nitrate conditions showed higher concentrations and a shallower depth of the nitracline at 2°–8°N (white dashed lines in Fig. 3e). In the 20°N transect, the lowest average nitrate concentration ( $0.87 \pm 0.37 \mu\text{mol L}^{-1}$ ) in the upper

300 m was found in the region of the eastern Luzon Strait. The patterns of  $\text{NH}_4^+$ ,  $\text{PO}_4^{3-}$ , and  $\text{SiO}_3^{2-}$  generally followed the trend of the nitrate concentrations in the water masses (Yu et al. unpubl. data).

The Chl *a* concentrations at the incubation stations are shown in Fig. 3e,f. Along the 130°E transect, the surface Chl *a*

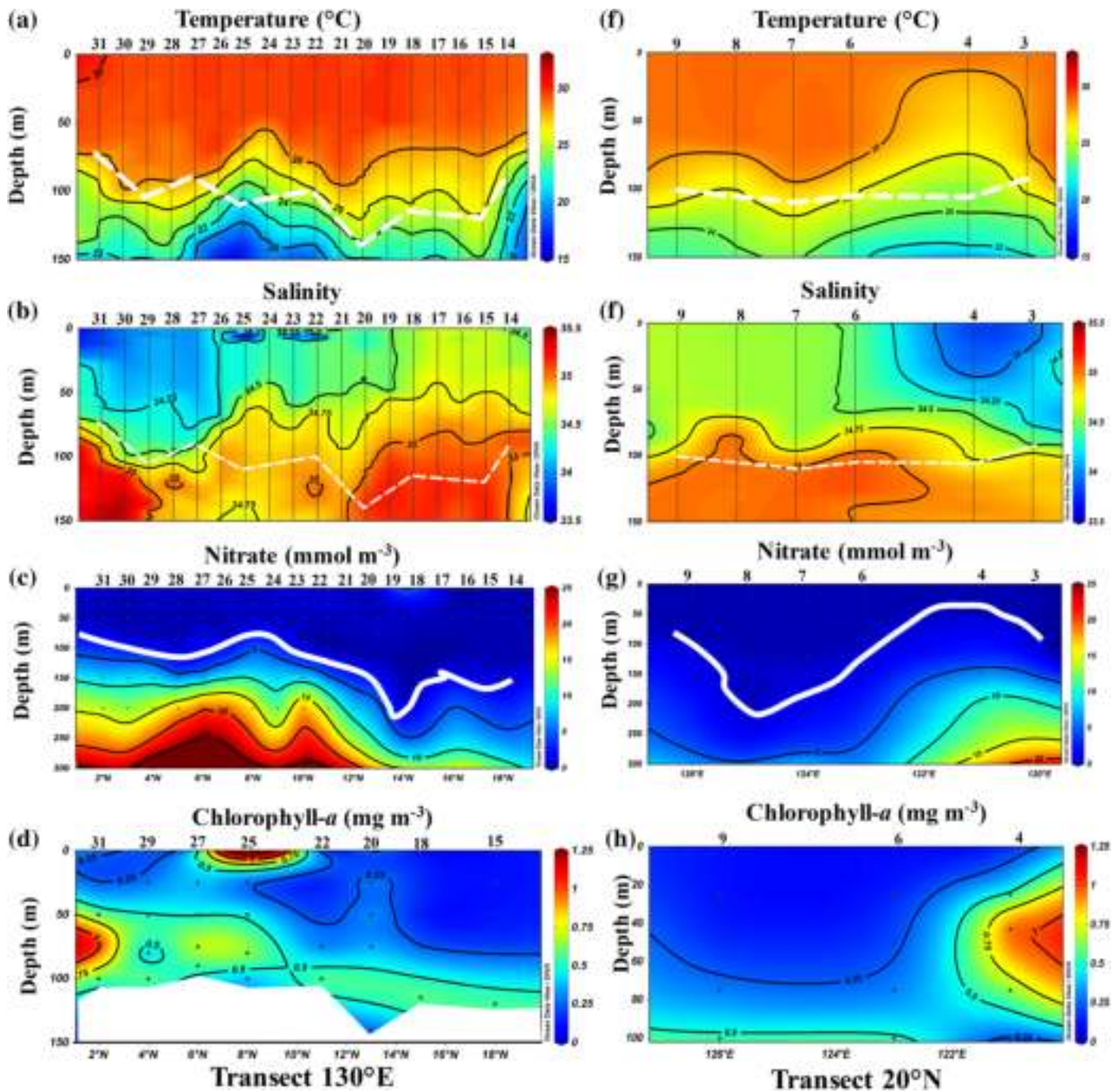


**Fig. 3.** Vertical distributions of temperature, salinity, nitrate, and Chl *a* on the south–north transect along 130°E and the west–east transect along 20°N. The white dashed and white solid lines represent the bottom of the euphotic zone and the depth of the nitracline, respectively. The numbers above the figures indicate the sampling stations. [Color figure can be viewed at [wileyonlinelibrary.com](http://wileyonlinelibrary.com)]

concentrations were lower in the surface water ( $< 0.25 \text{ mg m}^{-3}$ ), except for the presence of high values at the surface at Sta. 27. A well-developed DCM was observed at the base of the euphotic zone. The Chl *a* concentrations at the DCM decreased to the north from  $1 \text{ mg m}^{-3}$  at Sta. 31 to less than  $0.5 \text{ mg m}^{-3}$  at Sta. 15. Along the 20°N transect, shallower DCMs were observed at approximately 50 m in the region

of the eastern Luzon Strait compared to the stations to the west.

**Plankton community metabolism along the two transects**

Along the 130°E transect, the volumetric GPP ranged between 0.1 and  $1.2 \text{ mmol O}_2 \text{ m}^{-3} \text{ d}^{-1}$  and generally decreased with depth (Fig. 4a). Higher volumetric GPPs were found in the region of

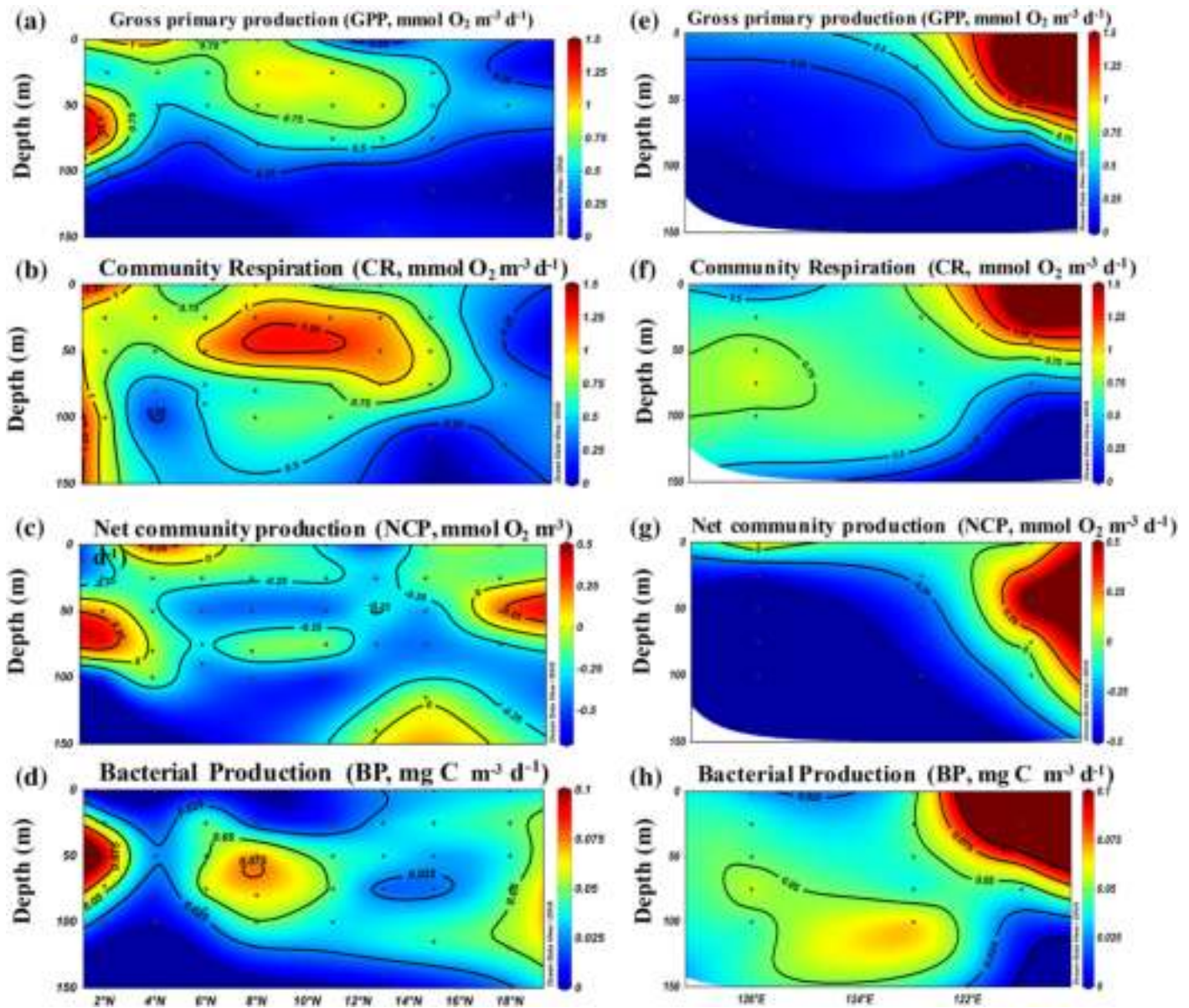


**Fig. 4.** Vertical distributions of volumetric GPP, CR, NCP, and BP along two transects (130°E and 20°N) in the western Pacific Ocean. The numbers above the figures indicate the sampling stations. [Color figure can be viewed at [wileyonlinelibrary.com](http://wileyonlinelibrary.com)]

2°–8°N (Sta. 25–31) and were associated with high nitrate and Chl *a* concentrations. The range of volumetric CRs was similar to that of the volumetric GPP, and the highest volumetric CR was located at the surface at Sta. 31 (Fig. 4b). The vertical gradient of CR was relatively homogenous along this transect (Fig. 4b). The volumetric NCP varied from  $-0.6 \text{ mmol O}_2 \text{ m}^{-3} \text{ d}^{-1}$  at the surface at Sta. 20 to  $0.4 \text{ mmol O}_2 \text{ m}^{-3} \text{ d}^{-1}$  at 70 m at Sta. 31 (Fig. 4c). Positive volumetric NCPs were mainly located in some surface and subsurface waters at low latitudes (Sta. 25–31; Fig. 4c). In terms of the euphotic zone integrated metabolism, the integrated GPP generally decreased to the north with higher values in the region of 2°–8°N (Fig. 5a). The spatial variation of the integrated CR had a similar pattern to that of the GPP although with a smaller

amplitude (Fig. 5b). The  $\text{O}_2$  integrated NCPs at Sta. 31 and 29 were close to zero, whereas a persistent net heterotrophic state was found from 5°N to 20°N (Fig. 5c).

For the 20°N transect, the maximum volumetric GPP ( $2.3 \text{ mmol O}_2 \text{ m}^{-3} \text{ d}^{-1}$ ) was coincident with the occurrence of the maximum volumetric CR ( $2.1 \text{ mmol O}_2 \text{ m}^{-3} \text{ d}^{-1}$ ) at the surface at Sta. 4 (Fig. 4e), where the waters were mixed by relatively nutrient-rich seawater from the adjacent South China Sea. At Sta. 6 and 9, which were affected by the oligotrophic KC, the volumetric GPP decreased to very low values, whereas the volumetric CR remained at intermediate values (Fig. 4e,f). As a result, positive volumetric NCP was observed throughout the water column at Sta. 4, and negative NCP was observed at Sta. 6 and 9 (Fig. 4g).

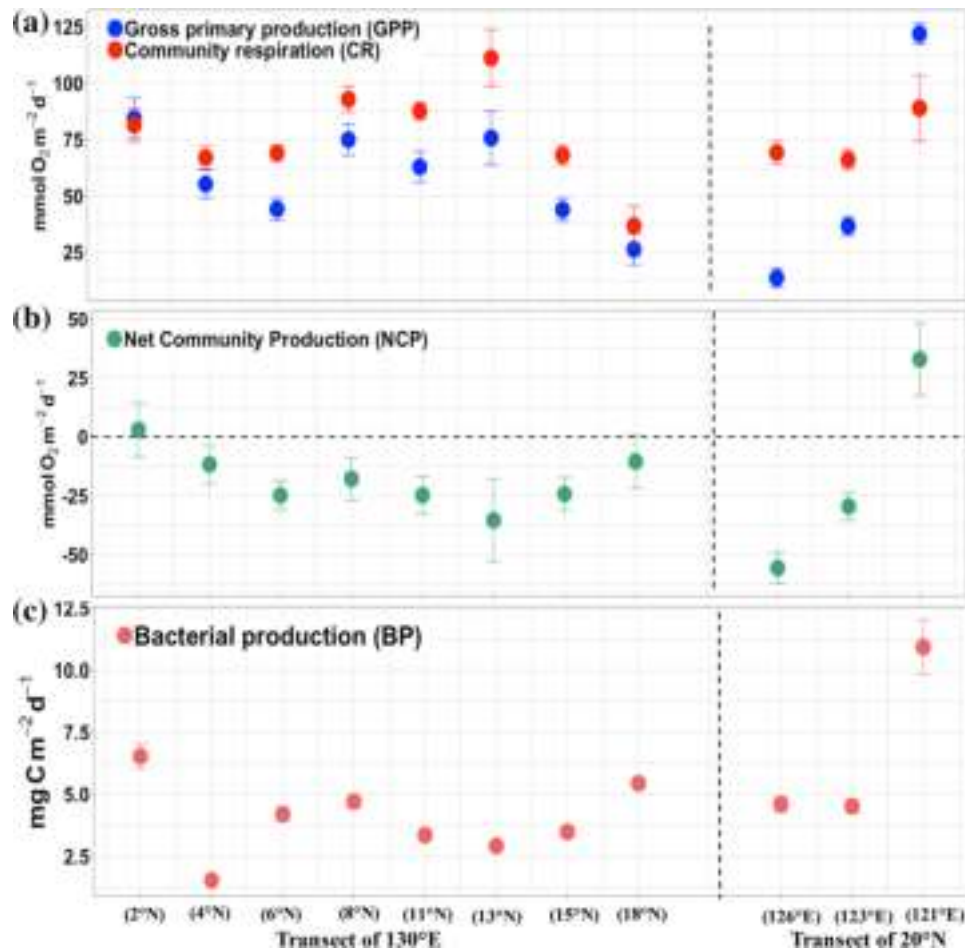


**Fig. 5.** Spatial variations of integrated (a) GPP and CR, (b) NCP, and (c) BP along the north–south transect at 130°E and the east–west transect at 20°N in the western Pacific Ocean. The error bars represent the standard error of the measurements. [Color figure can be viewed at [wileyonlinelibrary.com](http://wileyonlinelibrary.com)]

The euphotic zone integrated GPP decreased to the east along this transect from 122 mmol O<sub>2</sub> m<sup>-2</sup> d<sup>-1</sup> at the westernmost station to 13 mmol O<sub>2</sub> m<sup>-2</sup> d<sup>-1</sup> at the easternmost station (Fig. 5a). The range of the euphotic zone integrated CR in this transect was only one-third of the GPP, ranging from 66 mmol O<sub>2</sub> m<sup>-2</sup> d<sup>-1</sup> at Sta. 9 to 96 mmol O<sub>2</sub> m<sup>-2</sup> d<sup>-1</sup> at Sta. 4 (Fig. 5b). The integrated NCP showed pronounced shifts from a net autotrophic state at Sta. 4 to heterotrophic at Sta. 6 and 9 (Fig. 5c).

In general, the pooled data set for these two transects suggests that the spatial variation of GPP was greater than that of CR, which is reflected by the larger coefficient of variation of the integrated GPP (52%) than that of CR (27%). The euphotic zone integrated GPP was positively correlated with the integrated Chl *a* ( $r = 0.76$ ,  $p = 0.011$ ; Table 2, Fig. 6a) and the nitrate gradient across the base of the euphotic zone ( $r = 0.70$ ,  $p = 0.001$ ; Table 2, Fig. 6b). The CR can be regressed to GPP using the Equations  $CR = 1.15 * GPP^{0.74}$  ( $r^2 = 0.53$ ,  $p < 0.001$ ; Fig. 6c) for the volumetric values and  $CR = 11.74 * GPP^{0.48}$  ( $r^2 = 0.50$ ,  $p = 0.03$ ; Fig. 6d) for the integrated values. The slopes of the equations for GPP and CR indicate that the CR rates were slightly higher than the GPP; therefore, negative NCP prevailed at most of the stations. Based on the relationship

between the GPP and CR, the thresholds of the euphotic zone integrated and volumetric GPP (below which the system is net heterotrophic) were 110 mmol O<sub>2</sub> m<sup>-2</sup> d<sup>-1</sup> and 1.7 mmol O<sub>2</sub> m<sup>-3</sup> d<sup>-1</sup>, respectively.

### Bacterial production

Along the 130°E transect, the volumetric BP varied between 0.01 and 0.076 mg C m<sup>-3</sup> d<sup>-1</sup> with a mean value of 0.056 mg C m<sup>-3</sup> d<sup>-1</sup> (Fig. 4d). We observed maxima of the volumetric BP in the intermediate layer along this transect (Fig. 4d). Along the 20°N transect, the volumetric BP at the eastern stations tended to be lower than those at the western stations (Fig. 4h). The maximum volumetric BP of 0.53 mg C m<sup>-3</sup> d<sup>-1</sup> was found at the surface at Sta. 4, which was consistent with the maximum volumetric GPP and CR (Fig. 4h). In terms of depth-integrated values, the integrated BP did not show a pronounced spatial pattern in either the latitudinal or meridional transects (Fig. 5c). Except for the two peak values at Sta. 31 and 4, the integrated BPs along the two transects were both relatively constant and had intermediate values (Fig. 5c). The correlation between the integrated GPP and BP for the pooled dataset of the two transects was insignificant (Pearson  $p = 0.06$ ).

**Table 2.** Pearson correlations of the integrated metabolic rates with environmental variables ( $n = 11$ ).

|            | $\int$ Chl <i>a</i> | Surface Chl <i>a</i> | SST           | SS                   | Nitrate gradient    | $\int$ CR           | $\int$ NCP          | $\int$ BP    |
|------------|---------------------|----------------------|---------------|----------------------|---------------------|---------------------|---------------------|--------------|
| $\int$ GPP | <b>0.76 (0.011)</b> | 0.41 (0.212)         | 0.08 (0.819)  | <b>-0.68 (0.020)</b> | <b>0.65 (0.002)</b> | <b>0.70 (0.015)</b> | <b>0.72 (0.013)</b> | 0.63 (0.064) |
| $\int$ CR  | 0.47 (0.148)        | 0.41 (0.216)         | 0.23 (0.497)  | -0.25 (0.461)        | 0.28 (0.351)        | —                   | 0.01 (0.968)        | 0.14 (0.679) |
| $\int$ NCP | 0.57 (0.066)        | 0.14 (0.678)         | -0.11 (0.750) | <b>-0.72 (0.012)</b> | <b>0.68 (0.013)</b> | —                   | —                   | 0.41 (0.208) |
| $\int$ BP  | 0.30 (0.372)        | -0.01 (0.995)        | -0.43 (0.186) | -0.41 (0.215)        | -0.11 (0.742)       | —                   | —                   | —            |

$\int$ BP, integrated bacterial production rate;  $\int$ Chl *a*, integrated chlorophyll *a*;  $\int$ CR, community respiration;  $\int$ GPP, gross primary production;  $\int$ NCP, net community production; SS, surface salinity; SST, surface temperature.

The  $p$  values are shown in the brackets. The significant relationships are shown in bold ( $p < 0.05$ ).

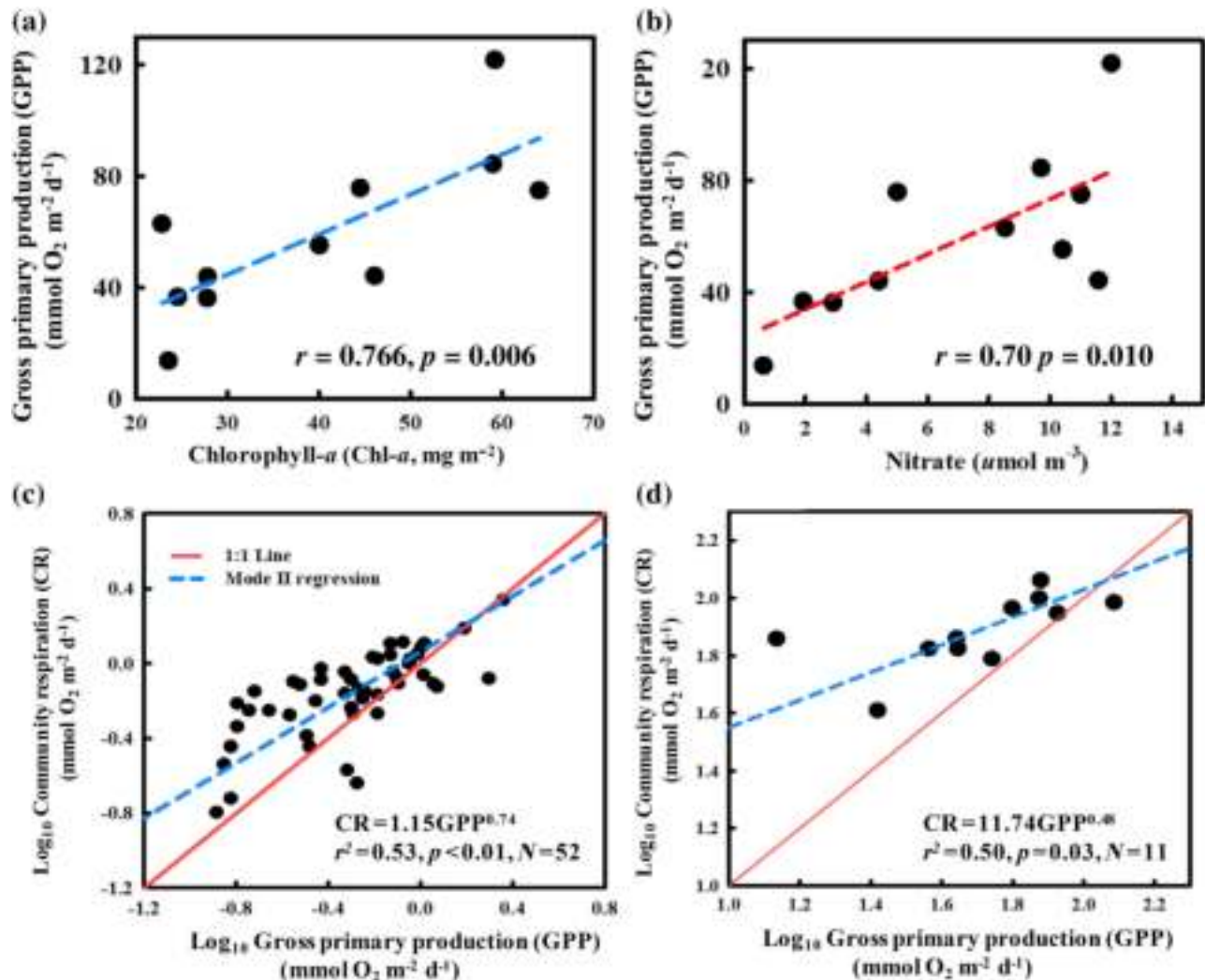


**Fig. 6.** (a) Pearson correlation between integrated GPP and integrated chlorophyll *a* (Chl *a*). (b) Pearson correlation between integrated GPP and average nitrate concentration in the upper 300 m. (c) Regression between volumetric GPP and CR. (d) Regression between integrated GPP and CR in the western Pacific Ocean. [Color figure can be viewed at [wileyonlinelibrary.com](http://wileyonlinelibrary.com)]

#### Comparison of metabolism estimates derived from the in vitro incubations, geochemical model, and empirical estimation

A comparison of the integrated metabolism derived from the in vitro incubations and the geochemical model along the

two transects is presented in Fig. 7. In general, the model of Letscher and Moore (2017) predicted moderate autotrophy in this region during September and October, with an average NCP of  $7 \text{ mmol O}_2 \text{ m}^{-2} \text{ d}^{-1}$  (Fig. 7a). By contrast, our measurements indicated a prevalence of net heterotrophic conditions in

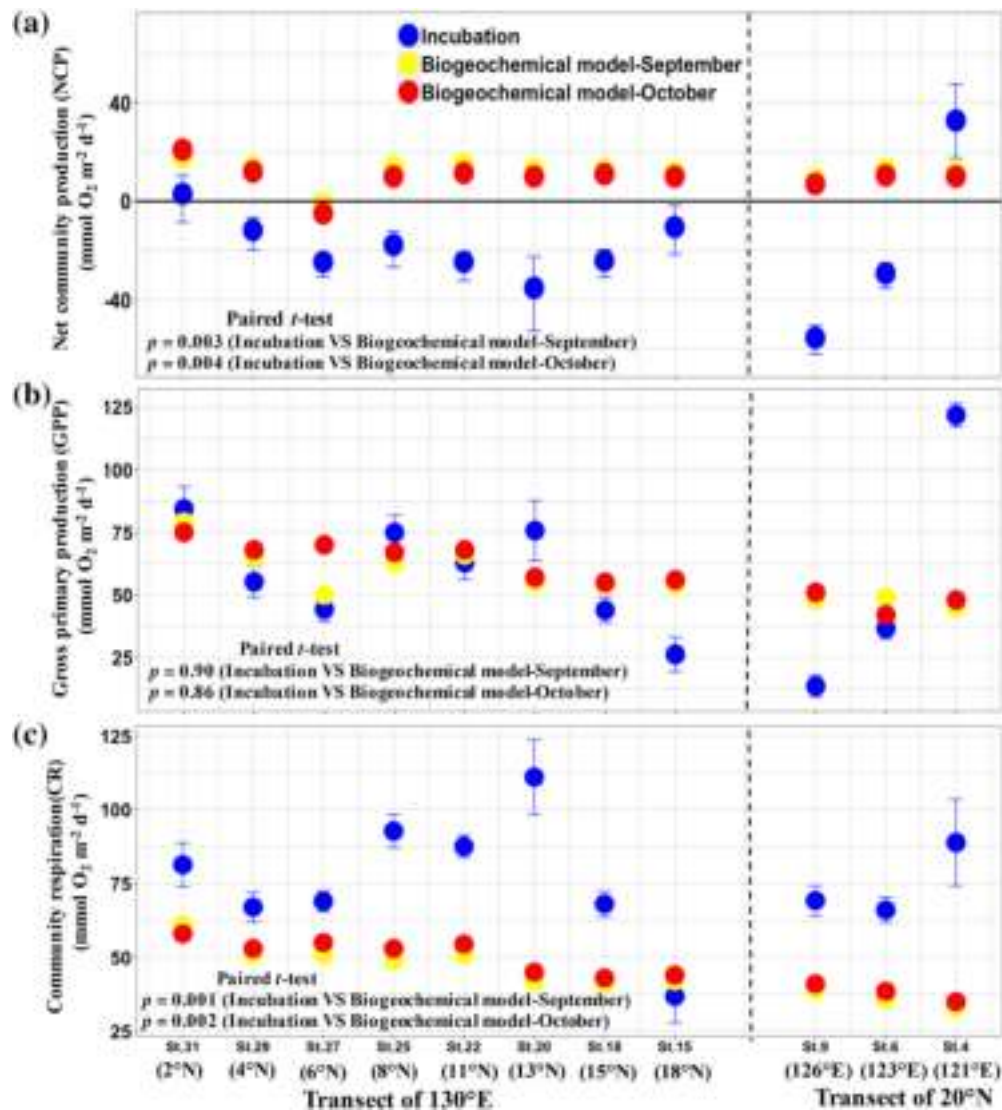


**Fig. 7.** Comparison between the integrated metabolism of (a) NCP, (b) GPP, and (c) CR at each sampling station derived from  $O_2$ -based incubation and the geochemical model of Letscher and Moore (2017). The  $p$  values shown in the figure were derived from the paired  $t$ -test. [Color figure can be viewed at [wileyonlinelibrary.com](http://wileyonlinelibrary.com)]

this region (Fig. 7a). Similar to our field observations of higher metabolism rates at low latitudes, the GPPs predicted from the geochemical model had slightly higher values at the low latitude stations, although the spatial variability was less pronounced than our field observations (Fig. 7b). The GPPs estimated from the geochemical model along the two transects ranged from 42 to 67  $\text{mmol } O_2 \text{ m}^{-2} \text{ d}^{-1}$ , yielding no statistical differences with the GPPs measured by  $O_2$ -based incubation ( $p = 0.90$  for the model output in September and  $p = 0.86$  for the model output in October, paired  $t$ -test; Fig. 7b). However, our field-observed CRs were statistically higher than those predicted by the geochemical model during September (paired  $t$ -test,  $p < 0.001$ ) and October (paired  $t$ -test,  $p < 0.001$ ; Fig. 7c).

The comparison of the CRs from the empirical estimates and the oxygen-based incubation approach showed that at

8 of the 11 stations, the measured CR exceeded the upper boundary of the empirical CR estimates, leaving a mean of 24  $\text{mmol } O_2 \text{ m}^{-2} \text{ d}^{-1}$  of respiration unaccounted for in this region (Fig. 8). Conversely, most of the CRs predicted by the biogeochemical model of Letscher and Moore (2017) fell within the range of values derived from the empirical estimations (Fig. 8).

## Discussion

The limited and uneven geographic distributions of the measured metabolic rates in the global ocean and reconciling the results of the metabolic balance derived from the incubation approach and the biochemical budget in a meaningful way remain major obstacles to a comprehensive understanding

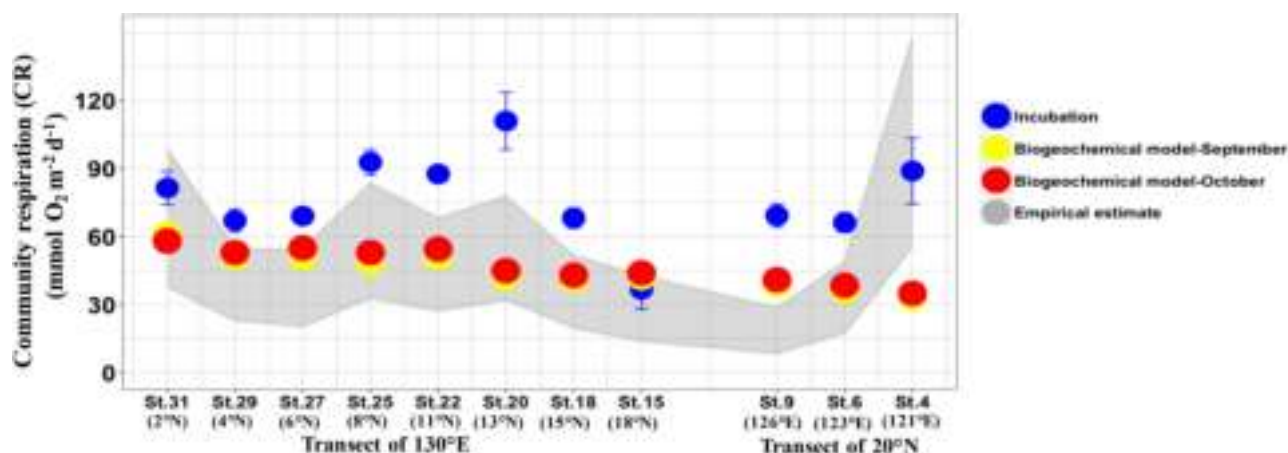


**Fig. 8.** Comparison of the CR derived from O<sub>2</sub>-based incubation, empirical estimates, and the geochemical model of Letscher and Moore (2017). The shade indicates the lower and upper boundaries of CR derived from empirical estimates. [Color figure can be viewed at [wileyonlinelibrary.com](http://wileyonlinelibrary.com)]

of the trophic status in the oligotrophic ocean (Westberry et al. 2012; Ducklow and Doney 2013). This study contributes to the currently limited data set in the western boundary currents of the North Pacific Ocean and, and more broadly, adds insight into the unresolved debate about the autotrophy vs. heterotrophy in the oligotrophic ocean.

#### Discrepancy of the regional metabolic state between the incubation and geochemical model predictions

The comparisons between the regional metabolic rates from the incubation approach and the model outputs address our first question. As we expected, the observations based on the oxygen changes during incubation exhibited a prevalence of net heterotrophic states in the warm and oligotrophic western Pacific Ocean. More than 80% of the volumetric NCP values were negative (Fig. 4c,g), and 8 of the 11 stations showed net heterotrophic states integrated over the entire water column (Fig. 5c). In this region, the environmental conditions feature high surface temperatures (> 28°C) and very low nutrient availability in the upper layers (Fig. 3). The mean Chl *a* and volumetric GPP were only approximately 0.14 mg m<sup>-3</sup> and 1.6 mmol O<sub>2</sub> m<sup>-3</sup> d<sup>-1</sup>, respectively, which fall into the conditions for a heterotrophic state according to the scaling laws proposed by Duarte et al. (2013).

However, the model of Letscher and Moore (2017) predicted a moderately autotrophic state in the western Pacific Ocean (Fig. 7a), which supports the metabolic state in the oligotrophic ocean that has been diagnosed by incubation-free methods in many previous studies (Emerson 2014; Yang et al. 2017a). Further comparisons of GPP and CR imply that our measured GPP values were consistent with the geochemistry-based values, but there was an apparent anomaly in the CR between these two approaches (Fig. 7b,c). At the global scale, the validity of gross O<sub>2</sub> production rates has been tested in numerous studies by comparing concurrent measurements of primary production determined from <sup>14</sup>C incorporation

(Michael et al. 1987; Grande et al. 1989; Bender et al. 1999). These results suggest that the GPP measured from in vitro O<sub>2</sub> change incubation generally tracks the distributions of <sup>14</sup>C-based primary production and could represent the true rates of autotrophic production. In this study, our measured GPPs were consistent with the changes in nutrient availability and Chl *a* concentrations at regional scales (Fig. 6a,b). In the broader Pacific Ocean, our regional mean GPP values (59.8 ± 8.7 mmol O<sub>2</sub> m<sup>-2</sup> d<sup>-1</sup>) were similar to the primary production in the central gyre of the North Pacific, which has similarly oligotrophic conditions (61 ± 5.9 mmol O<sub>2</sub> m<sup>-2</sup> d<sup>-1</sup>; Williams et al. 2004), but were significantly lower than the corresponding rates previously reported in the eastern equatorial Pacific (211 ± 64 mmol O<sub>2</sub> m<sup>-2</sup> d<sup>-1</sup>; Wambeke et al. 2008) and western subarctic Pacific (78 ± 24 mmol O<sub>2</sub> m<sup>-2</sup> d<sup>-1</sup>; Furuya (1995)), as determined by similar approaches. This latitudinal tendency of the GPP reflected by oxygen-based incubation is consistent with the current knowledge of higher nutrient availability in the colder and well-mixed Arctic water and the widespread occurrence of upwelling systems in the equatorial ocean, which adds further evidence of the rationality of GPP measurements at both regional and latitudinal scales.

In contrast to the consistency of the GPP between the incubation and biogeochemical model outputs, most of the CRs derived from the incubation approach exceeded the model predictions (Fig. 7c). In addition to the locally produced organic carbon (Fig. 7c), the model simulation of Letscher and Moore (2017) explicitly included the fluxes of semi-labile organic carbon and the lateral supply of allochthonous and terrigenous organic carbon, which are considered a key pathway to fuel the respiration if the prevalent heterotrophy is real. The apparent CR anomaly implies that in vitro estimates of CR are difficult to reconcile from the perspective of biogeochemical cycles. Unlike primary production, for which several independent incubation approaches (i.e., <sup>14</sup>C-based incorporation rates) can be used to constrain the global magnitude and

trends, it appears that there is no comparable incubation approach to directly measure the CR except for the oxygen consumption in dark bottles. Similar to many previous studies that showed the relative constancy of the geographical patterns of CR (Morán et al. 2004; Aranguren-Gassis et al. 2011; Wang et al. 2014), our depth-integrated CRs tended to be less variable than the GPPs, which casts further doubt on the accuracy of CR measurements.

### Reconciling the signal of CR determined by the incubation

The comparison between the incubation results and model outputs appears to support our GPP measurements, but it leaves some doubts about the magnitude of the in vitro CR. To further validate the CR between the model output and incubation approach, we performed another independent estimate of the respiration contributed by the major trophic groups of plankton at each station (Table 1) with the goal of constraining the possible CR based on the magnitude of the measured GPP and BP. Heterotrophic bacteria have long been considered to perform most of the respiration in the open ocean; therefore, individual measurements of BP are also a key factor influencing the magnitudes of our empirical CR estimates. The average rates of BP in our study region were at the low end of previously reported values in the Pacific systems and other oligotrophic systems (Table 3). The calculated BP requires a CF to transform the leucine incorporation rates into carbon production. Low leucine incorporation rates are typically found in oligotrophic, subtropical waters, and our measured leucine incorporation rates were comparable with the values in the oligotrophic ocean in ALOHA (Viviani and Church 2017). Therefore, the major possible cause of low BP might be related to the CF of leucine to carbon. In many previous studies, an empirical value of the leucine-to-carbon CF (i.e., 1.5 kg C mol leu<sup>-1</sup>) was used assuming no isotopic dilution (Kirchman 1993). Growing experimental evidence suggests that CF depends in part on the composition of the substrates and the nutrient status and that it decreases markedly from the coastal areas to the open ocean (Zubkov et al. 2000b; Alonso-Sáez et al. 2007). Our measured CF values (average of 0.37 kg C mol Leu<sup>-1</sup>) are well within the range of measured CFs in the oligotrophic system (Zubkov et al. 2000b;

Alonso-Sáez et al. 2007; Vázquez-Domínguez et al. 2008), which further indicates that the application of theoretical values of CF may potentially overestimate the bacterial activity in the oligotrophic ocean.

We found that an appreciable amount of measured CR could not be completely explained by the sum of the independent assessments of the different trophic groups at most of the stations (Fig. 8). Although considerable errors are associated with the CR estimates for each group, the results showed that even under the conditions of the maximum possible contribution, it is still difficult to bridge the gap between the in vitro measured respiration and the estimated respiration. Interestingly, most of the CRs predicted by the geochemical model fell within the possible range of the empirically estimated CRs, which in turn provides cross-validation of the rationality of the CR predicted by the geochemical model (Fig. 8). This analysis thus reveals that in vitro measurements of CR, rather than GPP measurements, are most likely responsible for the observation of net heterotrophy in this area. A similar finding was reported by Morán et al. (2007), who demonstrated that in the North Atlantic gyre, approximately 48% of the measured CR from changes in oxygen in dark bottles could not be explained by the contributions of trophic groups of plankton. The author related this discrepancy to the fundamental flaw associated with long-term dark incubation (24 h) in an enclosed system. Several previous studies highlighted the diel synchrony of the growth of photosynthetic prokaryotes in cultures and the ocean (Zubkov et al. 2000a; Jacquet et al. 2001). Long-term dark incubation might disrupt the diel synchrony of the dominant community of picoplankton. In spite of the still unclear consequences of this effect, it is likely that rapid disruption of the diel synchrony would lead to an elevation of the metabolic cost (i.e., respiration) for picoplankton under stress. Increases in bacterial abundances and substrate assimilation rates during bottle incubation have been revealed due to the exclusion of large zooplankton that feed on microheterotrophs, especially in oligotrophic systems characterized by tightly coupled microbial communities (Pomeroy et al. 1994; Evelyn et al. 1999). This effect of eliminating large predators in respiration measurements would be more apparent in the size-fraction incubation when > 1 μm organisms were removed, yielding a 50% overestimation of respiration in the bottle (Aranguren-Gassis et al. 2012). In addition,

**Table 3.** Review of euphotic zone integrated bacterial metabolism (mean ± SE) in the Pacific Ocean, adjacent ocean, and subtropical oceans.

| Region                    | Leu incorporation<br>(pmol m <sup>-2</sup> h <sup>-1</sup> ) | Leu CF<br>(kg C mol <sup>-1</sup> Leu <sup>-1</sup> ) | Bacterial production<br>(mg C m <sup>-2</sup> d <sup>-1</sup> ) | References                |
|---------------------------|--|---|---|---------------------------|
| Northern Pacific gyre     | 739 ± 140  | 1.5   | 27 ± 2.1  | Viviani and Church (2017) |
| Eastern South Pacific     | 4360 ± 1200  | 1.5   | 160 ± 46  | Wambeke et al. (2008)     |
| Western subarctic Pacific | 1572 ± 740   | 1.06  | 40 ± 14   | Sherry et al. (2002)      |
| Northern South China Sea  | 3941 ± 1200  | 0.37  | 35 ± 7.2  | Wang et al. (2014)        |
| Northern Atlantic gyre    | 958 ± 123  | 0.73  | 17 ± 2.3  | Morán et al. (2007)       |
| Western Pacific boundary  | 627 ± 260  | 0.37  | 5.6 ± 1.2   | This study                |

“new surfaces” for bacterial attachment in the container may be favorable for the growth of attached bacteria, enhancing respiration during bottle incubation. However, the precise mechanism of the overestimation of CR by in vitro incubations is beyond the scope of our current data. A useful caveat of our study might be a request to further check the possible methodological problem, especially that associated with dark incubation.

## Conclusion

This study is the first to report plankton community and bacterial metabolism on the western boundary of the northern Pacific Ocean based on in vitro incubation. The combination of analyses across different approaches allows us to enhance our understanding of the metabolic state of the oligotrophic ocean, particularly in the interpretation of net heterotrophy determined from light–dark bottles. Our comparison with the biogeochemical model and the contributions of major plankton groups suggests that the negative NCP may stem from systematically overestimated in vitro measured CR, although the exact cause of the problem is unresolved and requires further study.

## References

- Alonso-Sáez, L., J. M. Gasol, J. Arístegui, J. C. Vilas, D. Vaqué, C. M. Duarte, and S. Agustí. 2007. Large-scale variability in surface bacterial carbon demand and growth efficiency in the subtropical northeast Atlantic Ocean. *Limnol. Oceanogr.* **52**: 533–546. doi:10.4319/lo.2007.52.2.0533
- Aranguren-Gassis, M., P. Serret, E. Fernandez, J. L. Herrera, J. F. Domínguez, V. Perez, and J. Escanez. 2011. Production and respiration control the marine microbial metabolic balance in the eastern North Atlantic subtropical gyre. *Deep-Sea Res. Part I Oceanogr. Res. Pap.* **58**: 768–775. doi:10.1016/j.dsr.2011.05.003
- Aranguren-Gassis, M., E. Teira, M. Serret, S. Martínez-García, and E. Fernández. 2012. Potential overestimation of bacterial respiration rates in oligotrophic plankton communities. *Mar. Ecol. Prog. Ser.* **453**: 1–10. doi:10.3354/meps09707
- Arrigo, K. R. 2005. Erratum: Marine microorganisms and global nutrient cycles. *Nature* **437**: 349–348. doi:10.1038/nature04158
- Azam, F., T. Fenchel, J. G. Field, J. S. Gray, L. A. Meyerreil, and F. Thingstad. 1983. The ecological role of water-column microbes in the sea. *Mar. Ecol. Prog. Ser.* **10**: 257–263. doi:10.3354/meps010257
- Bender, M., J. Orchardo, M.-L. Dickson, R. Barber, and S. Lindley. 1999. *In vitro* O<sub>2</sub> fluxes compared with <sup>14</sup>C production and other rate terms during the JGOFS Equatorial Pacific experiment. *Deep-Sea Res. Part I Oceanogr. Res. Pap.* **46**: 637–654. doi:10.1016/S0967-0637(98)00080-6
- Bjørnsen, P. K., and J. Kuparinen. 1991. Determination of bacterioplankton biomass, net production and growth efficiency in the Southern Ocean. *Mar. Ecol. Prog. Ser.* **71**: 185–194. doi:10.3354/meps071185
- Calbet, A., and M. R. Landry. 2004. Phytoplankton growth, microzooplankton grazing, and carbon cycling in marine systems. *Limnol. Oceanogr.* **49**: 51–57. doi:10.4319/lo.2004.49.1.0051
- Carvalho, M. C., K. G. Schulz, and B. D. Eyre. 2017. Respiration of new and old carbon in the surface ocean: Implications for estimates of global oceanic gross primary productivity. *Global Biogeochem. Cycles* **31**: 975–984. doi:10.1002/2016GB005583
- Chen, B., B. Huang, Y. Xie, C. Guo, S. Song, L. I. Hongbo, and H. Liu. 2014. The bacterial abundance and production in the East China Sea: Seasonal variations and relationships with the phytoplankton biomass and production. *Acta Oceanol. Sin.* **33**: 166–177. doi:10.1007/s13131-014-0528-0
- Clarke, G. L., and R. H. Oster. 1934. The penetration of the blue and red components of daylight into Atlantic coastal water and its relation to phytoplankton metabolism. *Biol. Bull.* **67**: 59–75. doi:10.2307/1537482
- R Core Team. 2014. A language and environment for statistical computing. R Foundation for Statistical Computing.
- Del Giorgio, P. A., J. J. Cole, and A. Cimleris. 1997. Respiration rates in bacteria exceed phytoplankton production in unproductive aquatic systems. *Nature* **385**: 148–151. doi:10.1038/385148a0
- Duarte, C. M., and J. Cebrián. 1996. The fate of marine autotrophic production. *Limnol. Oceanogr.* **41**: 1758–1766. doi:10.4319/lo.1996.41.8.1758
- Duarte, C. M., A. Regaudie-de-Gioux, J. M. Arrieta, A. Delgado-Huertas, and S. Agustí. 2013. The oligotrophic ocean is heterotrophic. *Ann. Rev. Mar. Sci.* **5**: 551–569. doi:10.1146/annurev-marine-121211-172337
- Ducklow, H. W., and S. C. Doney. 2013. What is the metabolic state of the oligotrophic ocean? A debate. *Ann. Rev. Mar. Sci.* **5**: 525–533. doi:10.1146/annurev-marine-121211-172331
- Emerson, S. 2014. Annual net community production and the biological carbon flux in the ocean. *Global Biogeochem. Cycles* **28**: 14–28. doi:10.1002/2013gb004680
- Evelyn, B. S., F. S. Barry, and T. S. Crystal. 1999. Activity of marine bacteria under incubated and in situ conditions. *Aquat. Microb. Ecol.* **20**: 213–223. doi:10.3354/ame020213
- Field, C. B., M. J. Behrenfeld, J. T. Randerson, and P. Falkowski. 1998. Primary production of the biosphere: Integrating terrestrial and oceanic components. *Science* **281**: 237–240. doi:10.1126/science.281.5374.237
- Fine, R. A., R. Lukas, F. M. Bingham, M. J. Warner, and R. H. Gammon. 1994. The western equatorial Pacific: A water mass crossroads. *J. Geophys. Res. Oceans* **99**: 25063–25080. doi:10.1029/94JC02277
- Fenchel, T., and B. J. Finlay. 1983. Respiration rates in heterotrophic, free-living protozoa. *Microb. Ecol.* **9**: 99–122. doi:10.1007/BF02015125

- Fukuda, R., H. Ogawa, T. Nagata, and I. Koike. 1998. Direct determination of carbon and nitrogen contents of natural bacterial assemblages in marine environments. *Appl. Environ. Microbiol.* **64**: 3352–3358.
- Furuya, O. A. 1995. Primary production and community respiration in the subarctic water of the western North Pacific, p. 239–253. *In* Biogeochemical processes and ocean flux in the Western Pacific. Terra Scientific Publishing.
- Grande, K. D., P. J. L. Williams, J. Marra, D. A. Purdie, K. Heinemann, R. W. Eppley, and M. L. Bender. 1989. Primary production in the North Pacific gyre: A comparison of rates determined by the  $^{14}\text{C}$ ,  $\text{O}_2$  concentration and  $^{18}\text{O}$  methods. *Deep-Sea Res. Part A Oceanogr. Res. Pap.* **36**: 1621–1634. doi:10.1016/0198-0149(89)90063-0
- Hedges, J. I., J. A. Baldock, Y. Gélinas, C. Lee, M. L. Peterson, and S. G. Wakeham. 2002. The biochemical and elemental compositions of marine plankton: A NMR perspective. *Mar. Chem.* **78**: 47–63. doi:10.1016/S0304-4203(02)00009-9
- Hu, D., and others. 2015. Pacific western boundary currents and their roles in climate. *Nature* **522**: 299–308. doi:10.1038/nature14504
- Huang, Y., and others. 2018. Effects of increasing atmospheric  $\text{CO}_2$  on the marine phytoplankton and bacterial metabolism during a bloom: A coastal mesocosm study. *Sci. Total Environ.* **633**: 618–629. doi:10.1016/j.scitotenv.2018.03.222
- Jacquet, S., F. Partensky, J. F. Lennon, and D. Vaultot. 2001. Diel patterns of growth and division in marine picoplankton in culture. *J. Phycol.* **37**: 357–369. doi:10.1046/j.1529-8817.2001.037003357.x
- Jiao, N., and others. 2010. Microbial production of recalcitrant dissolved organic matter: Long-term carbon storage in the global ocean. *Nat. Rev. Microbiol.* **8**: 593–599. doi:10.1038/nrmicro2386
- Kirchman, D. 1993. Leucine incorporation as a measure of biomass production by heterotrophic bacteria, p. 509–512. *In* P. F. Kemp, B. F. Sherr, E. B. Sherr, and J. J. Cole [eds.], *In Handbook of methods in aquatic microbial ecology*. Lewis Publishers.
- Kyewalyanga, M., T. Platt, and S. Sathyendranath. 1992. Ocean primary production calculated by spectral and broad-band models. *Mar. Ecol. Prog. Ser.* **85**: 171–185. doi:10.3354/meps085171
- Laws, E. A. 1991. Photosynthetic quotients, new production and net community production in the open ocean. *Deep-Sea Res. Part A Oceanogr. Res. Pap.* **38**: 143–167. doi:10.1016/0198-0149(91)90059-0
- Laws, E. A., G. R. DiTullio, K. L. Carder, P. R. Betzer, and S. Hawes. 1990. Primary production in the deep blue sea. *Deep-Sea Res. Part A Oceanogr. Res. Pap.* **37**: 715–730. doi:10.1016/0198-0149(90)90001-C
- Letscher, R. T., and J. K. Moore. 2017. Modest net autotrophy in the oligotrophic ocean. *Global Biogeochem. Cycles* **31**: 699–708. doi:10.1002/2016GB005503
- Longhurst, A. 1995. Seasonal cycles of pelagic production and consumption. *Prog. Oceanogr.* **36**: 77–167. doi:10.1016/0079-6611(95)00015-1
- López-Urrutia, Á., E. San Martín, R. P. Harris, and X. Irigoien. 2006. Scaling the metabolic balance of the oceans. *Proc. Natl. Acad. Sci. USA* **103**: 8739–8744. doi:10.1073/pnas.0601137103
- López-Urrutia, Á., and X. A. G. Morán. 2007. Resource limitation of bacterial production distorts the temperature dependence of oceanic carbon cycling. *Ecology* **88**: 817–822. doi:10.1890/06-1641
- Marra, J., and R. T. Barber. 2004. Phytoplankton and heterotrophic respiration in the surface layer of the ocean. *Geophys. Res. Lett.* **31**: L09314. doi:10.1029/2004GL019664
- Michael, B., and others. 1987. A comparison of four methods for determining planktonic community production. *Limnol. Oceanogr.* **32**: 1085–1098. doi:10.4319/lo.1987.32.5.1085
- Miller, J. C., and J. N. Miller. 1988. Analytical and Bioanalytical Chemistry, p. 1676–1677. *In* E. Howood [ed.], *Statistics for analytical chemistry*, v. **378**, 2nd ed. Great Britain Publishers.
- Morán, X. A. G., E. Fernández, and V. Pérez. 2004. Size-fractionated primary production, bacterial production and net community production in subtropical and tropical domains of the oligotrophic NE Atlantic in autumn. *Mar. Ecol. Prog. Ser.* **274**: 17–29. doi:10.3354/meps274017
- Morán, X. A. G., V. Pérez, and E. Fernández. 2007. Mismatch between community respiration and the contribution of heterotrophic bacteria in the NE Atlantic open ocean: What causes high respiration in oligotrophic waters? *J. Mar. Res.* **65**: 545–560. doi:10.1357/002224007782689102
- Oudot, C., R. Gerard, P. Morin, and I. Gningue. 1988. Precise ship-board determination of dissolved-oxygen (Winkler procedure) for productivity studies with a commercial system. *Limnol. Oceanogr.* **33**: 146–150. doi:10.4319/lo.1988.33.1.0146
- Pomeroy, L. R., J. E. Sheldon, and W. M. Sheldon Jr. 1994. Changes in bacterial numbers and leucine assimilation during estimations of microbial respiratory rates in seawater by the precision Winkler method. *Appl. Environ. Microbiol.* **60**: 328–332.
- Qu, T., H. Mitsudera, and T. Yamagata. 1999. A climatology of the circulation and water mass distribution near the Philippine Coast. *J. Phys. Oceanogr.* **29**: 1488–1505. doi:10.1175/15200485(1999)029<1488:ACOTCA>2.0.CO;2
- Regaudie-de-Gioux, A., and C. M. Duarte. 2012. Temperature dependence of planktonic metabolism in the ocean. *Global Biogeochem. Cycles* **26**: GB1015. doi:10.1029/2010GB003907
- Rivkin, R. B., and L. Legendre. 2001. Biogenic carbon cycling in the upper ocean: Effects of microbial respiration. *Science* **291**: 2398–2400. doi:10.1126/science.291.5512.2398
- Robinson, C., P. Serret, G. Tilstone, E. Teira, M. V. Zubkov, A. P. Rees, and E. M. S. Woodward. 2002. Plankton respiration in the Eastern Atlantic Ocean. *Deep-Sea Res. Part I Oceanogr. Res. Pap.* **49**: 787–813. doi:10.1016/S0967-0637(01)00083-8

- Robinson, C., and P. J. L. B. Williams. 2005. Chapter 9: Respiration and its measurement in surface marine waters, p. 147–181. In P. del Giorgio [ed.], *Respiration in aquatic ecosystems*. Oxford Univ. Press.
- Roland, F., and J. J. Cole. 1999. Regulation of bacterial growth efficiency in a large turbid estuary. *Aquat. Microb. Ecol.* **20**: 31–38. doi:10.3354/ame020031
- Schlitzer, R. 2012. Ocean data view; [accessed 2013 November 3]. Available from [odv.awi.de](http://odv.awi.de)
- Serret, P., E. Fernandez, J. A. Sostres, and R. Anadon. 1999. Seasonal compensation of microbial production and respiration in a temperate sea. *Mar. Ecol. Prog. Ser.* **187**: 43–57. doi:10.3354/meps187043
- Serret, P., and others. 2015. Both respiration and photosynthesis determine the scaling of plankton metabolism in the oligotrophic ocean. *Nat. Commun.* **6**: 6961. doi:10.1038/ncomms7961
- Sherry, N. D., B. Imanian, K. Sugimoto, P. W. Boyd, and P. J. Harrison. 2002. Seasonal and interannual trends in heterotrophic bacterial processes between 1995 and 1999 in the subarctic NE Pacific. *Deep-Sea Res. Part II Top. Stud. Oceanogr.* **49**: 5775–5791. doi:10.1016/S0967-0645(02)00214-X
- Shiozaki, T., K. Furuya, T. Kodama, and S. Takeda. 2009. Contribution of N<sub>2</sub> fixation to new production in the western North Pacific Ocean along 155°E. *Mar. Ecol. Prog. Ser.* **377**: 19–32. doi:10.3354/meps07837
- Sigman, D. M., and E. A. Boyle. 2000. Glacial/interglacial variations in atmospheric carbon dioxide. *Nature* **407**: 859–869. doi:10.1038/35038000
- Straile, D. 1997. Gross growth efficiencies of protozoan and metazoan zooplankton and their dependence on food concentration, predator-prey weight ratio, and taxonomic group. *Limnol. Oceanogr.* **42**: 1375–1385. doi:10.4319/lo.1997.42.6.1375
- Vázquez-Domínguez, E., C. M. Duarte, S. Agustí, K. Jürgens, D. Vaqué, and J. M. Gasol. 2008. Microbial plankton abundance and heterotrophic activity across the Central Atlantic Ocean. *Prog. Oceanogr.* **79**: 83–94. doi:10.1016/j.pocean.2008.08.002
- Verity, P. G. 1985. Grazing, respiration, excretion, and growth rates of tintinnids. *Limnol. Oceanogr.* **30**: 1268–1282. doi:10.4319/lo.1985.30.6.1268
- Viviani, D. A., and M. J. Church. 2017. Decoupling between bacterial production and primary production over multiple time scales in the North Pacific Subtropical Gyre. *Deep-Sea Res. Part I Oceanogr. Res. Pap.* **121**: 132–142. doi:10.1016/j.dsr.2017.01.006
- Wambeke, F. V., I. Obernosterer, T. Moutin, S. Duhamel, O. Ulloa, and H. Claustre. 2008. Heterotrophic bacterial production in the eastern South Pacific: Longitudinal trends and coupling with primary production. *Biogeosciences* **5**: 157–169. doi:10.5194/bg-5-157-2008
- Wang, N., W. Lin, B. Chen, and B. Huang. 2014. Metabolic states of the Taiwan Strait and the northern South China Sea in summer 2012. *J. Trop. Oceanogr.* **33**: 61–68 [in Chinese with English abstract].
- Welschmeyer, N. A. 1994. Fluorometric analysis of chlorophyll a in the presence of chlorophyll b and pheopigments. *Limnol. Oceanogr.* **39**: 1985–1992. doi:10.4319/lo.1994.39.8.1985
- Westberry, T. K., P. J. L. B. Williams, and M. J. Behrenfeld. 2012. Global net community production and the putative net heterotrophy of the oligotrophic oceans. *Global Biogeochem. Cycles* **26**, GB4019, doi:10.1029/2011GB004094
- Williams, P. J., P. D. Quay, T. K. Westberry, and M. J. Behrenfeld. 2013. The oligotrophic ocean is autotrophic. *Ann. Rev. Mar. Sci.* **5**: 535–549. doi:10.1146/annurev-marine-121211-172335
- Williams, P. J. L. B., P. J. Morris, and D. M. Karl. 2004. Net community production and metabolic balance at the oligotrophic ocean site, station ALOHA. *Deep-Sea Res. Part I Oceanogr. Res. Pap.* **51**: 1563–1578. doi:10.1016/j.dsr.2004.07.001
- Williams, P. J. L. B., and P. A. del Giorgio. 2005. In P. A. del Giorgio and P. J. L. B. Williams [eds.], *Respiration in aquatic ecosystems*. Oxford Univ. Press.
- Yang, B., S. R. Emerson, and S. M. Bushinsky. 2017a. Annual net community production in the subtropical Pacific Ocean from *in-situ* oxygen measurements on profiling floats. *Global Biogeochem. Cycles* **31**: 728–744. doi:10.1002/2016GB005545
- Yang, G., C. Li, K. Guilini, X. Wang, and Y. Wang. 2017b. Regional patterns of <sup>δ13</sup>C and <sup>δ15</sup>N stable isotopes of size-fractionated zooplankton in the western tropical North Pacific Ocean. *Deep-Sea Res. Part I Oceanogr. Res. Pap.* **120**: 39–47. doi:10.1016/j.dsr.2016.12.007
- Yang, G., C. Li, Y. Wang, X. Wang, L. Dai, Z. Tao, and P. Ji. 2017c. Spatial variation of the zooplankton community in the western tropical Pacific Ocean during the summer of 2014. *Cont. Shelf Res.* **135**: 14–22. doi:10.1016/j.csr.2017.01.009
- Zhou, H., D. Yuan, P. Guo, M. Shi, and Q. Zhang. 2010. Mesoscale circulation at the intermediate-depth east of Mindanao observed by Argo profiling floats. *Science China Earth Sciences* **53**: 432–440. doi:10.1007/s11430-009-0196-7
- Zubkov, M. V., M. A. Sleigh, and P. H. Burkill. 2000a. Assaying picoplankton distribution by flow cytometry of underway samples collected along a meridional transect across the Atlantic Ocean. *Aquat. Microb. Ecol.* **21**: 13–20. doi:10.3354/ame021013
- Zubkov, M. V., M. A. Sleigh, P. H. Burkill, and R. J. G. Leakey. 2000b. Bacterial growth and grazing loss in contrasting areas of North and South Atlantic. *J. Plankton Res.* **22**: 685–711. doi:10.1093/plankt/22.4.685

#### Acknowledgments

This study was supported by grants from the National Key Research and Development Program of China (No.2016YFA0601201), National Major Research Program of China (2015CB954002), the China NSF Projects (No.41330961, 41876009), and partially supported by the starter grant from University of Strathclyde (to B. Chen). Data acquisition and sample collections were supported by NSFC Open Research Cruise (Cruise

No.NORC2016-09 under grant of No. 41549909), which was conducted onboard R/V "KEXUE" by the Institute of Oceanography, Chinese Academy of Sciences, China. We also thank Dr. Xin Liu for the useful suggestions on data analysis.

*Submitted 30 June 2018*

*Revised 13 January 2019*

*Accepted 25 March 2019*

*Associate editor: Anya Waite*

**Conflict of Interest**

None declared.